Nonspecular x-ray scattering from multilayer structures

J. B. Kortright
Center for X-ray Optics, Lawrence Berkeley Laboratory, University of California, Berkeley, California 94720

(Received 22 March 1991; accepted for publication 28 June 1991)

Nonspecular x-ray ($\lambda = 0.154$ nm) scattering from a 3.9-nm-period tungsten/carbon multilayer structure with scattering vectors near low-angle multilayer specular interference peaks is reported. Diffuse intensity results from kinematical small-angle scattering from in-plane structural inhomogeneities associated with the individual interfaces or layers having characteristic length scales much greater than the multilayer period. Modulations in this diffuse nonspecular intensity when the incident or observation angle is equal to the angle of the first-order multilayer Bragg peak result from standing-wave-enhanced scattering and other dynamical effects. The technique provides a sensitive measure of in-plane structural inhomogeneities of heterointerface systems.

I. INTRODUCTION

Nanometer-period x-ray multilayer structures derive their utility primarily from the specular Bragg reflectance resulting from constructive interference of reflected amplitudes from each of the interfaces that make up these compositionally modulated structures.[1–3] Ideal multilayer specular reflectors would have composition or structural modulations only along the direction of the normal to the interfaces, would be homogeneous in the plane of the layers, and thus would exhibit only specular x-ray reflectance in the low-scattering-vector region near multilayer Bragg peaks. As is the case for x-ray reflectance from a single interface,[4] structural inhomogeneities in the plane of the interfaces of multilayer structures yield a diffuse, nonspecular component to the scattering, in addition to the specular component, characterized by scattering vectors away from the specular direction.[5–7] For the multilayer case, imperfections in the large number of interfaces (or ultrathin layers) enhance the nonspecular signal above that from a single interface (or layer). This paper demonstrates that high-quality multilayer specular x-ray reflectors exhibit measurable nonspecular scattering. Several distinct features of nonspecular intensity are observed, some of which have been observed previously from multilayer samples.[6,8–13] The distribution of these nonspecular features in the multilayer reciprocal space is described, and possible origins of these features are discussed.

II. EXPERIMENT

The multilayer studied here is representative of high-quality structures on high-quality substrates used in x-ray applications. It consists of 40 periods of alternating tungsten and carbon layers, with each period 39.0 Å thick. It was formed by dc magnetron sputtering onto a 1-in.-diam, superpolished, fused silica substrate flat to $\lambda/10$ (λ visible) having rms microroughness of less than 1 Å over a range of spatial wavelengths from 0.8 μm to 0.6 mm as measured by a WYKO optical profilometer. X-ray measurements were made using a 12-kW rotating anode generator with a Ge (111) monochromator providing a quasiparallel Cu$K\alpha_1$ beam to the sample at the axis of a two-circle diffractometer. A scintillator crystal/photomultiplier detected the radiation from the sample beyond a 0.5-mm slit 50 cm from the sample. The incident beam had a full-width at half-maximum (FWHM) of 0.125° and specular reflectance measurements were possible over 8 orders of magnitude. Data are normalized to a scale where the incident beam peak has intensity 1. Three types of angular scans were made and are defined in terms of the incident and observation angles θ_i and θ_o, which added equal the scattering angle 2θ as in Fig. 1(a). Specular scans have $\theta_i = \theta_o = \frac{1}{2}(2\theta)$ directing the scattering vector $\mathbf{q}$ along the sample normal (z direction). With $\theta_i \neq \theta_o$ asymmetric or nonspecular scans are made having $\mathbf{q}$ components both in the plane of the surface (q_x) and normal to this plane (q_z). Rocking scans vary θ_i with 2θ constant, and 2θ scans vary that angle with θ_i constant.

The measured intensity in a specular scan, shown in Fig. 2, exhibits many orders of multilayer Bragg peaks, confirming reasonably sharp composition gradients at the interfaces and a high degree of structural perfection. The weak even-order peaks indicate that the individual W- and C-rich layers make up roughly half of the 39.0-Å period. At these small angles refraction is relatively large and rapidly varying with angle. The apparent period d_m of the mth order is obtained using the measured peak angle θ_m from $m\lambda = 2d_m \sin\theta_m$, and is related to the actual period d by a first-order refraction correction,[14] $d_m = d(1 - \delta \csc^2\theta_m)$, where $1 - \delta = n$ is the effective real part of the complex index of refraction for the multilayer structure. Least-squares analysis of d_m vs $\csc^2\theta_m$ yields $d = 39.0 \pm 0.05$ Å and $\delta = 2.83 \times 10^{-5}$.

Calculating the trajectories of the three types of scans in multilayer reciprocal space aids in understanding the distribution and origins of the observed nonspecular intensity. This amounts to correcting for refraction to calculate the scattering vector $\mathbf{q}$ inside of the multilayer, and is accomplished by matching in-plane components of wave vec-

 0021-8979/91/073620-06$03.00

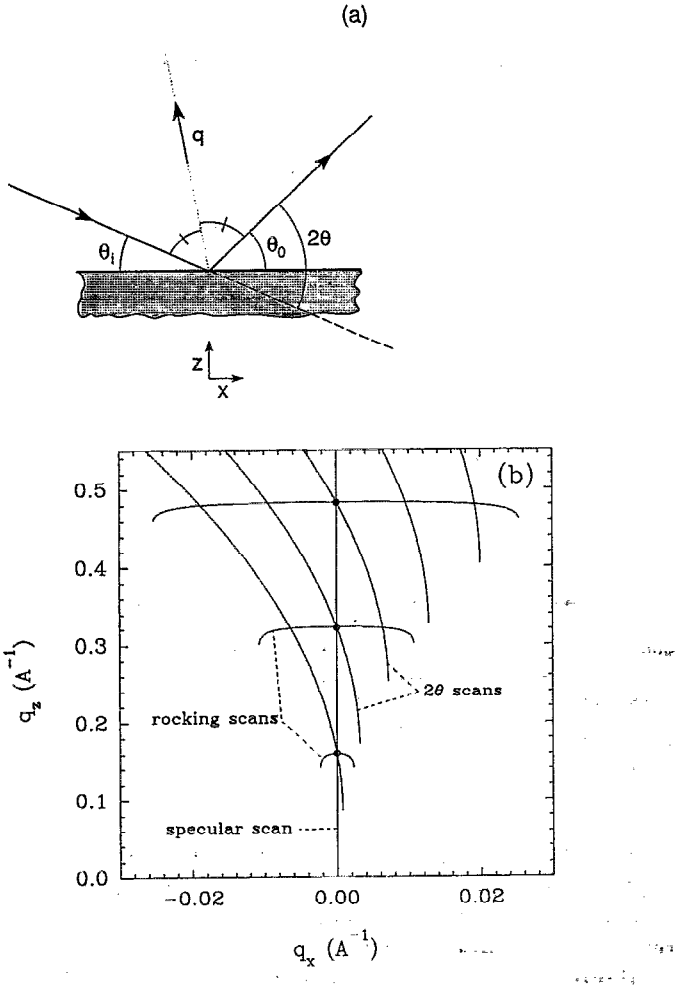

FIG. 1. (a) Scattering geometry used; the diffractometer varies the incident angle θ_i and the scattering angle 2θ. The observation angle $\theta_o = 2\theta - \theta_i$. (b) Angle scans through reciprocal space for this W/C multilayer passing through the multilayer Bragg peaks calculated using Eq. (1).

tors at the interfaces and using Snell's law to obtain

$$q_x = (2\pi/\lambda)\,(\cos\theta_o - \cos\theta_i), \tag{1}$$

$$q_z = (n2\pi/\lambda)[(1 - \cos^2\theta_i/n^2)^{1/2} + (1 - \cos^2\theta_o/n^2)^{1/2}].$$

No assumptions of small θ or δ are made, so these expressions are valid into the extreme ultraviolet range where these quantities may not be small. n is obtained from the specular scan as above, and q_z is real except when either θ_i or θ_o is less than the critical angle for total external reflection $\theta_c = (2\delta)^{1/2}$, in which case q_z is complex and only evanescent fields exist in depth into the sample. Figure 1(b) shows trajectories through reciprocal space of the three types of scans. The line at $q_x = 0$ corresponds to the specular scan in Fig. 2; the equally spaced points along this line are the multilayer Bragg peaks at $q_z = m(0.161\ \text{Å}^{-1})$, $m = 1,2,3,\ldots$. With this refraction correction, θ_c corresponds to $q_z = 0$ in the specular scan. The predominantly horizontal lines correspond to rocking scans; at the extremities of these scans refraction causes significant reduction in q_z. The rocking scans shown pass through the multilayer reciprocal lattice points. 2θ scans

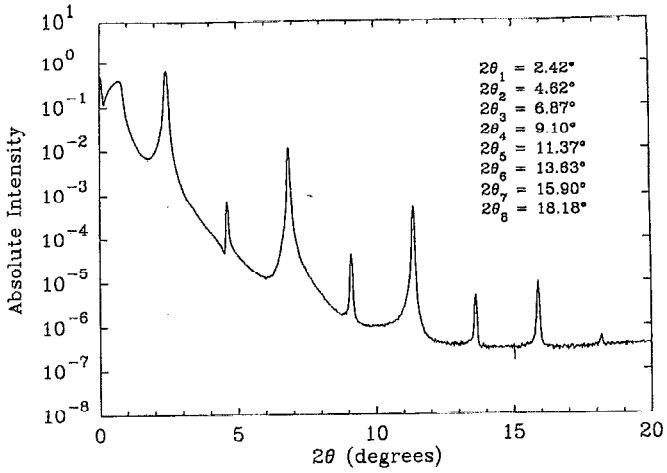

FIG. 2. Specular reflectance from W/C multilayer vs grazing incidence angle showing many orders of Bragg reflection. The sample does not intercept the entire beam until the grazing incidence angle is nearly 1°, accounting for the shape of the total reflection region. Angular positions of the Bragg peaks are noted.

through these points are the diagonal lines in the figure. In 2θ scans q_z varies rapidly and q_x slowly. The end points of the scan trajectories correspond to angular positions at which either θ_i or θ_o equals θ_c. The range of q_x available for measurement (i.e., where θ_i and $\theta_o > \theta_c$) is proportional to $q_z^{1/2}$, limiting the range of correlations from which in-plane scattering can be measured as $q_z \to 0$.

III. RESULTS AND DISCUSSION

A diffuse, nonspecular intensity above the background scattering level is observed over the entire range of $\mathbf{q}$ available for measurement. Several features in the nonspecular scattering are evident from a series of closely spaced rocking and 2θ scans in the region from $q_z = 0$ through the third-order multilayer reciprocal lattice point and near the fifth-order point. In Fig. 3 these features are clearly observed in the series of rocking scans across the first- , second- , and third-order reciprocal lattice points.

The most prominent nonspecular features are diffuse streaks directed along q_x at constant q_z corresponding to reciprocal lattice points. Concentrating on the feature near the third-order peak in Fig. 3(c) this diffuse intensity extends in $|q_x|$ from 0 to the limit set by θ_c, and is most intense for the rocking scan that passes through the Bragg peak ($2\theta_3 = 6.87°$). For scans with $2\theta \leqslant 2\theta_3$ this diffuse intensity decreases monotonically with $|q_x|$ (except for two sharp modulations, which are discussed below), while for scans with $2\theta > 2\theta_3$ this diffuse intensity increases at large $|q_x|$. These shapes are explained by the trajectories of rocking scans through reciprocal space, together with additional information from a series of 2θ scans across this feature at many fixed θ_i values. Each 2θ scan has a peak whose angular positions are plotted in reciprocal space in Fig. 4, and form streaks directed along q_x at constant q_z corresponding to the third-order reciprocal lattice points. The sets of rocking scans in Fig. 3(c) traverse this linear

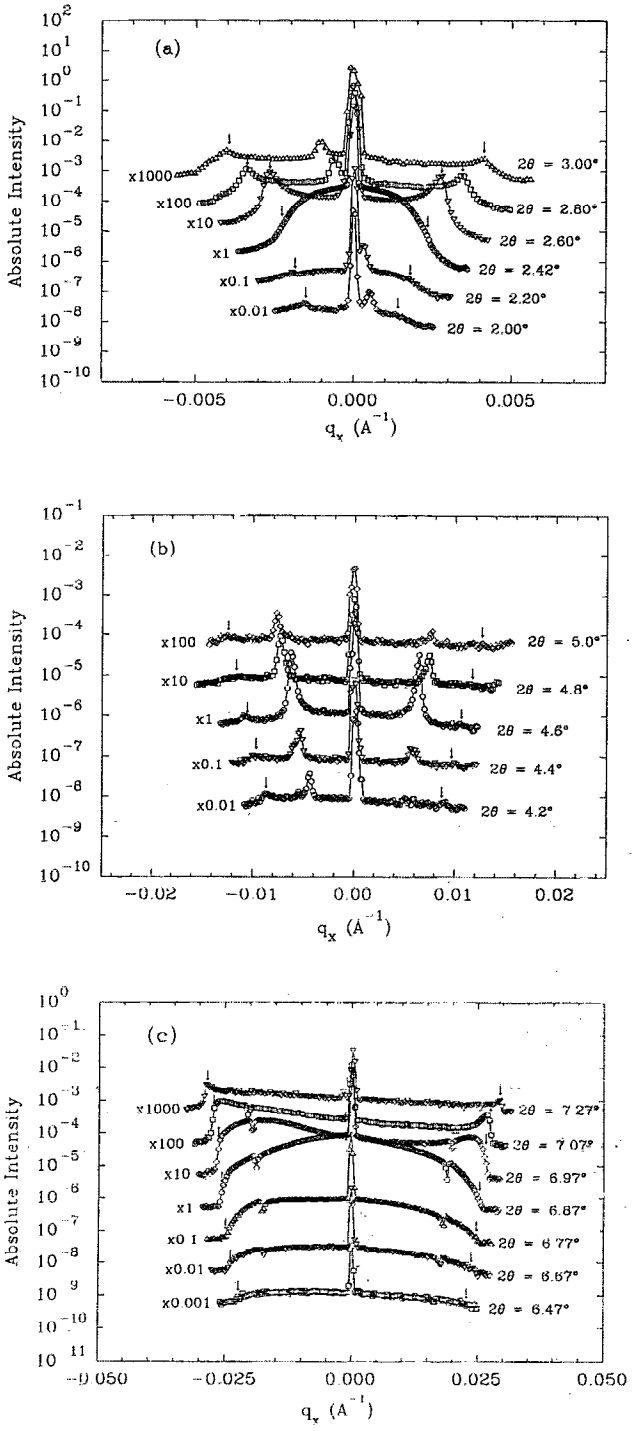

FIG. 3. Rocking scans at different 2θ values near the first-, second-, and third-order multilayer Bragg peaks are in (a), (b), and (c), respectively. q_x rather than θ_i is the ordinate so the specular peak always falls at $q_x = 0$. In each plot the rocking scan passing closest to the Bragg spot is plotted on the absolute intensity scale, while adjacent scans are offset by an order of magnitude for clarity. Near the extremities of each scan a vertical arrow marks the position where either θ_i or θ_o equals θ_c. The extreme data points in each scan define the background counting rate.

feature in the curved trajectory shown in Fig. 1(b), accounting for the changing shape of these rocking scans with 2θ. Even though the q_x and q_z scales in Fig. 4 are different, the width of these diffuse intensity features in

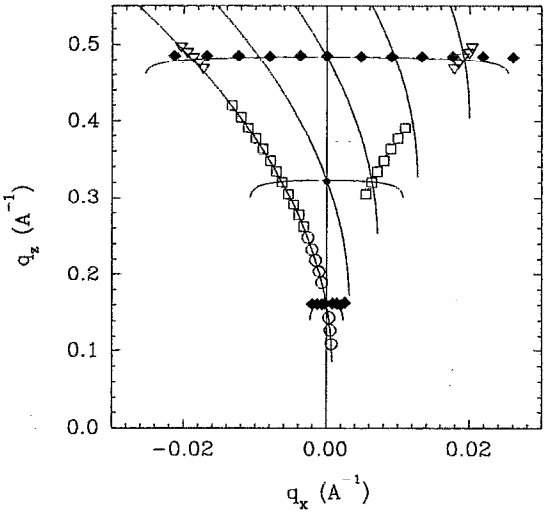

FIG. 4. Positions of features of nonspecular scattering in multilayer reciprocal space. Measured peaks in 2θ scans are shown as ♦ and represent diffuse streaks at constant q_z. Peaks in rocking scans are ○ and □ and form ridges of intensity when either θ_i or $\theta_o = \theta_1$. Dips in rocking scans are ▽ and form valleys at these same conditions. Lines are trajectories of rocking, 2θ, and specular scans through reciprocal lattice points as in Fig. 1(b).

q_x near the third-order spot is several times the width in q_z, which is roughly equal to that of the third-order specular peak. Thus the diffuse intensity associated with the Bragg peaks is not isotropically distributed around the third-order peak, but is directed along q_x. Similar streaks of diffuse intensity are associated with the first- and fifth-order Bragg peaks. Weaker diffuse intensity exists at q_z values away from Bragg points. Since these nonspecular streaks are most intense about multilayer Bragg peaks, their origin is linked to the multilayer structure itself.

This nonspecular scattering results from structural inhomogeneities associated with the individual interfaces or layers that make up the multilayer, and is analogous to small-angle scattering from lateral imperfections within the multilayer structure. Detailed analysis of the width and shape in q_x of this nonspecular intensity requires correction for an asymmetric resolution function and an absorption correction and will be presented in a future paper. Several general observations are made here. The diffuse streaks along q_x are peaked at $q_x = 0$. This suggests, following understanding gained in the analysis of small-angle scattering from condensed samples,[15] that the scattering centers that form these heterogenieties either are present in very low concentration, or have no preferred periodicities in their distribution that would be expected to give rise to oscillations or maxima in the intensity along q_x. Near the third-order peak the uncorrected half-width of the distribution in q_x is of order 0.01 Å^{-1}. Significant diffuse intensity extends to $|q_x| \simeq 0.03$ Å^{-1}, the limit set by θ_c. Near the fifth-order peak, the uncorrected half-width is roughly 0.02 Å^{-1}, and diffuse intensity extends over $|q_x|$ to at least 0.072 Å^{-1}. Without rigorous analysis it is impossible to obtain quantitative values describing structural attributes

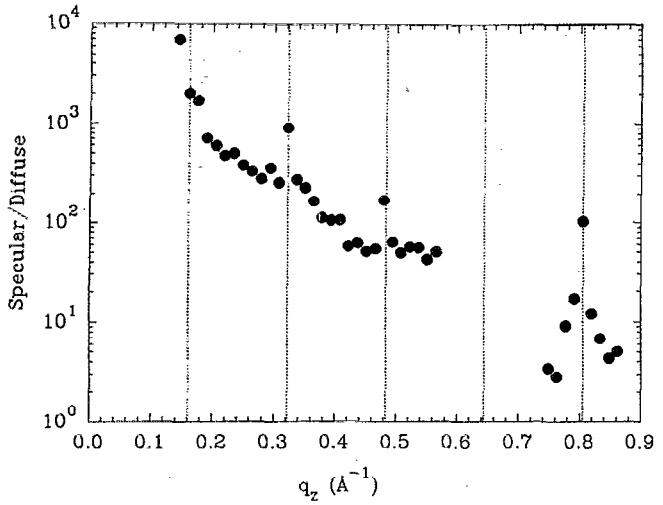

FIG. 5. The ratio of the peak specular intensity to the peak diffuse intensity (measured at the base of the specular peak) shows a strong dependence on q_z. Vertical lines indicate the positions of the first five multilayer Bragg peaks.

of the heterogeneities. However, using the concept that the width of the distribution in q_x is inversely proportional to a characteristic dimension in the x-y plane, we infer that a characteristic dimension yielding this nonspecular intensity is of order $2\pi/(0.02\ \text{Å}^{-1}) = 314$ Å, roughly an order of magnitude greater than the thickness of the individual layers of this structure.

The ratio of the specular to peak diffuse intensity is a strong function of q_z, as seen in Fig. 5. This ratio shows roughly exponential dependence on q_z away from $q_z = m2\pi/d$, where it has values above this dependence. The peaks in this ratio at Bragg points show that the diffuse component does not exhibit the same degree of multilayer enhancement as does the specular component, which results from the coherent Bragg reflectance process in which the reflectance is enhanced by roughly the square of the number of interfaces. The existence of diffuse streaks along q_x at the Bragg points shows that the nonspecular component does exhibit some multilayer enhancement. For q_z near the first-order peak the specular component of scattering is dominant, while near the fifth-order peak the peak diffuse intensity is nearly as strong as the specular component. Considering that the diffuse component extends much farther in q_x than the specular component, the integrated diffuse intensity is greater than the integrated specular intensity at larger q_z. Therefore, when $|\mathbf{q}| \simeq 2\pi/d$ the scattering is primarily specular in nature, and as $|\mathbf{q}|$ increases the scattering becomes more nonspecular in character. Since this is a relatively high-quality x-ray multilayer structure, the heterogeneities within the individual layers or interfaces presumably have dimensions less than d projected along $\mathbf{q}$, which is directed at most several degrees away from the z direction for these measurements. This is consistent with a predominant specular component for small $|\mathbf{q}|$ near the first Bragg peak, where the scattering vector couples to the multilayer period d, and a growing nonspecular component as $|\mathbf{q}|$ increases into the range matched with features having dimensions less than d.

While it is clear that inhomogeneities in the x-y plane cause this directed, diffuse nonspecular intensity, here we only speculate as to the nature of in-plane structural inhomogeneities. Imperfections in the substrate may propagate into the multilayer stack. While this cannot be ruled out, the substrate used here is of the highest optical quality available to minimize any contribution to structural inhomogeneities from the substrate. The inhomogeneities may be intrinsic to the layers themselves, reflecting imperfect layering or interface formation during the multilayer growth process, or microstructural heterogeneities within the individual layers. Theoretical models describing scattering from rough surfaces generally assume an interface between two well-defined media described by a height–height correlation function.[4–6] For multilayers of interest here individual layers are of order 1 nm, or only several atom layers, thick. Evidence of intermixing at interfaces exists,[16] and transmission electron microscopy (TEM) studies reveal in-plane inhomogeneities within the individual layers which may not be best described as roughness at a well-defined interface.[17] Structural imperfections may take the form of rough interfaces, or may be heterogeneities within the individual layers, in which case the assumption of interfaces between well-defined media may not be a realistic description for nanometer-scale multilayers.

The in-plane inhomogeneities may or may not be correlated from one layer to the next.[5,6,13,18] Perfect correlation of roughness from one layer to the next would result in a multilayer in which the roughness of the substrate is mapped conformally along z to each interface above it. Uncorrelated roughness would describe a structure in which imperfections in each interface (or layer) have no correlation in z from layer to layer. Savage *et al.*[13] recently argue that diffuse streaks along q_x at Bragg points, as observed here, necessarily imply a high degree of correlated or conformal roughness. These authors do not fully justify this conclusion. It is clear that enhanced nonspecular scattering is observed when $q_z = m2\pi/d$. It is also clear that correlated roughness is expected to give rise to these diffuse peaks. To see this we can think of correlated roughness as a lateral mosaic structure within the multilayer, which would result in multilayer Bragg peaks spread over the angular width of the mosaic spread at constant $|\mathbf{q}|$. However, it does not follow that only correlated roughness causes these diffuse streaks. Even in the case of uncorrelated roughness in a periodic multilayer structure, there exists periodicity in the z direction imposed by the multilayer structure. The situation of "vertically random roughness" described in Ref. 13 does not exist in periodic multilayers; the imperfections in the z direction in the uncorrelated roughness case are random deviations away from the average multilayer periocidity. Multilayers are a set of rough interfaces or layers (correlated or not) distributed periodically in z, and thus the diffuse component, like the specular component, may show enhancement at the multilayer interference conditions simply because of the periodicity imposed by the multilayer. While there are

differences in the theoretical description of the scattering from correlated and uncorrelated roughness, existing theoretical work[5,6] does not preclude multilayer-enhanced nonspecular scattering from structures having uncorrelated roughness, and one paper supports this connection.[5] These scalar theoretical treatments were developed for laser light scattering from dielectric multilayers in the visible-light range. Application of rigorous vector theories is called for to further address this and other subtleties of nonspecular x-ray scattering from multilayer structures.

Other features in the nonspecular scattering are observed as modulations in this directed diffuse intensity which occur when θ_i or θ_o equal θ_1. Near the first-order Bragg peak [Fig. 3(a)] a weak nonspecular peak in rocking scans is observed at positive q_x when $2\theta < 2\theta_1$ and at negative q_x when $2\theta > 2\theta_1$, and corresponds to a ridge of intensity at $\theta_i = \theta_1$ (plotted as ○ in Fig. 4). This ridge through the first-order peak has been previously observed, and was interpreted to result from an assumed mosaic structure in the multilayer imposed by the substrate.[9] In this model individual mosaic blocks oriented away from the average specular direction exhibit multilayer Bragg reflection when $\mathbf{q}$ is oriented along the block normal. This model cannot explain the observed direction of the ridge in q space, since for a mosaic model each mosaic block would diffract with $\mathbf{q}$ of equal magnitude but with slightly different direction. Standing-wave-enhanced scattering[19] from the same in-plane inhomogeneities resulting in the streaked diffuse intensity can explain the ridge of intensity with $\theta_i = \theta_1$ passing through the first-order peak. Standing waves having the periodicity of the multilayer exist only when $\theta_i = \theta_1$. The electric-field amplitude of these standing waves can approach twice that of the incident beam. These enhanced fields would scatter from in-plane inhomogeneities with intensities greater than when $\theta_i \neq \theta_1$, accounting for the observed ridge through the first-order peak. The measured peak intensity along this ridge is roughly three times the diffuse background, consistent with the amount of enhancement obtainable with standing waves. Near the first-order Bragg peak this nonspecular ridge of intensity is observed only when θ_i (not θ_o) equals θ_1, consistent with the existence of standing waves only at this condition. This enhanced nonspecular scattering is similar to that observed when $\theta_i = \theta_c$ (the Yoneda effect).[20–23]

At q_z values near the second- and third-order Bragg peaks, modulations in rocking scans are observed symmetrically about $q_x = 0$ when either θ_i or θ_o equals θ_1 [Figs. 3(b) and 3(c)]. Near the second-order Bragg peak these modulations form ridges in the nonspecular intensity (plotted as □ in Fig. 4), while near the third-order Bragg peak they form valleys (plotted as ▽ in Fig. 4). The symmetric distribution of these features indicates that they are not standing-wave-enhanced diffuse scattering as near the first peak, but rather result from other dynamical effects. The peaks in the ridge of intensity along θ_i and $\theta_0 = \theta_1$ occur when $2\theta \simeq 2\theta_2$, or when $\mathbf{q}$ has roughly the same value it has at the second-order peak. Evidently multiple scattering accounts for these peaks by a mechanism in which nonspecular q_x components couple the first- and second-order Bragg conditions. The peak at $\theta_i = \theta_1$ and $2\theta = 2\theta_2$ is observed over a larger range of q_z than the peak at $\theta_o = \theta_1$ and $2\theta = 2\theta_2$ because the q_z resolution is asymmetric in q_x. The valleys near the third-order peak at θ_i or $\theta_o = \theta_1$ must result from a similar dynamical effect resulting in decreased intensity. These symmetric valleys are not simply the result of removal of photons available for nonspecular scattering when the first-order Bragg condition is satisfied, since this would only explain the valley at $\theta_i = \theta_1$, not both.

IV. SUMMARY

In summary, nonspecular x-ray scattering can be measured from high-quality multilayer structures on high-quality substrates within a limited range of q_x. Diffuse intensity directed in the plane of the layers arises from structural inhomogeneities within the interfaces or layers having correlation lengths much greater than the thickness of the individual layers. Ridges and valleys in the diffuse intensity are observed when θ_i or θ_o equal θ_1, and arise from several different dynamical effects. None of these features would be observed if the multilayer studied were perfectly homogeneous in the x-y plane. These general features were observed for several different x-ray multilayer structures on similar substrates (including Mo/Si multilayers).

The observed nonspecular scattering has implications for applications of multilayers as x-ray optical elements and for the characterization of in-plane inhomogeneities in heterostructures in general. Regarding x-ray optical applications, these measurements are equivalent to measuring the point-spread function of this multilayer structure which is related to the Fourier transform of the modulation transfer function of this reflective optic. Such measurements are therefore useful in estimating the limitations of imaging performance imposed by structural imperfections within the multilayer.[24] For the multilayer structure studied here, the diffuse nonspecular intensity is several orders less than the specular reflectance at the first peak, confirming that the diffuse component from high-quality multilayers on high-quality substrates should not significantly limit imaging performance. More generally, the imperfections resulting in nonspecular scattering also reduce the specular intensity. Nonspecular scattering provides a direct measure of structural imperfections within the multilayer, and can therefore be used to monitor the effect of varying growth conditions on the structure and properties of small-period multilayers structures. Similar nonspecular scattering measurements, albeit with weaker intensity, may be a useful probe of structural imperfections associated with the formation of single heterointerfaces. A more intense source, such as a synchrotron, together with increased signal-to-background ratio, would permit weaker nonspecular features to be observed. Extracting detailed information regarding the nature of in-plane structural inhomogeneities from measured scattering will require further theoretical development using realistic models for these structures. Further work in this area is underway.

ACKNOWLEDGMENTS

The author acknowledges discussions with E. Gullikson, C. Lucas, D. Stearns, P. Dhez, and Y. Wu. This work was supported by the Director, Office of Energy Research, Office of Basic Energy Sciences, Materials Sciences Division, of the U.S. Department of Energy under Contract No. AC03-76SF00098.

[1] E. Spiller, AIP Conf. Proc. **75**, 124 (1981).
[2] T. W. Barbee, AIP Conf. Proc. **75**, 131 (1981).
[3] J. H. Underwood and T. W. Barbee, Appl. Opt. **20**, 3027 (1981).
[4] S. K. Sinha, E. B. Sirota, S. Garoff, and H. B. Stanley, Phys. Rev. B. **38**, 2297 (1988), and references therein.
[5] J. M. Eastman, in *Physics of Thin Films, Advances in Research and Development*, edited by G. Hass and M. H. Francombe (Academic, New York, 1978), p. 167.
[6] J. M. Elson, J. Pl Rahn, and J. M. Bennett, Appl. Opt. **19**, 669 (1980).
[7] D. G. Stearns, J. Appl. Phys. **65**, 491 (1989).
[8] A. Brunson, C. Dufour, B. George, M. Vergnat, C. Marchal, and P. Mangin, Solid State Commun. **71**, 1045 (1989).
[9] F. E. Christensen, A. Hornstrup, P. Frederiksen, P. Grundsoe, S. Henrichsen, E. Jaconsen, P. Jonasson, M. M. Madsen, C. Hilsson, H. W. Schnopper, N. J. Westerfaard, and P. Orup, J. X-ray Sci. Technol. **2**, 81 (1990).
[10] H. Homma, Y. Lepetre, U. M. Murduck, I. K. Shuller, and C. F. Majkrzak, Proc. Int. Soc. Opt. Eng. **563**, 150 (1985).
[11] J. Corno, E. Dartyge, P. Dhez, A. Fontaine, J. Jucha, Y. Lepetre, and B. Pardo, Proc. Int. Soc. Opt. Eng. **733**, 398 (1986).
[12] M. F. Toney (private communication).
[13] D. E. Savage, J. Kleiner, N. Schimke, Y. H. Phang, T. Jankowsky, J. Jacobs, R. Dariotis, and M. G. Lagally, J. Appl. Phys. **69**, 1411 (1991).
[14] R. W. James, *The Optical Principles of the Diffraction of X-rays* (Ox Bow, Woodbridge, CT, 1982).
[15] A. Guinier and G. Fournet, *Small-Angle Scattering of X-rays* (Wiley, New York, 1955).
[16] J. B. Kortright and J. D. Denlinger, MRS Symp. Proc. **103**, 95 (1988).
[17] T. D. Nguyen, R. Gronsky, and J. B. Kortright, MRS Symp. Proc. **139**, 357 (1989); **187**, 95 (1990).
[18] D. L. Rosen, D. Brown, J. Gilfrich, and P. Burkhalter, J. Appl. Cryst. **21**, 136 (1988).
[19] J. B. Kortright and A. Fischer-Colbrie, J. Appl. Phys. **61**, 1130 (1987).
[20] Y. Yoneda, Phys. Rev. **131**, 2010 (1963).
[21] B. E. Warren and J. S. Clarke, J. Appl. Phys. **36**, 324 (1965).
[22] O. J. Geuntert, J. Appl. Phys. **36**, 1361 (1965).
[23] A. N. Nigam, Phys. Rev. **138**, A1189 (1965).
[24] J. E. Harvey, E. C. Moran, and W. P. Zmek, Appl. Opt. **27**, 1527 (1988).